

This document contains a post-print version of the paper

An integrated thermal model of hot rolling

authored by **Katrin Speicher, Andreas Steinboeck, Daniel Wild, Thomas Kiefer, and Andreas Kugi**
and published in *Mathematical and Computer Modelling of Dynamical Systems*.

The content of this post-print version is identical to the published paper but without the publisher's final layout or copy editing. Please, scroll down for the article.

Cite this article as:

K. Speicher, A. Steinboeck, D. Wild, T. Kiefer, and A. Kugi, "An integrated thermal model of hot rolling", *Mathematical and Computer Modelling of Dynamical Systems*, vol. 20, no. 1, pp. 66–86, 2014. DOI: [10.1080/13873954.2013.809364](https://doi.org/10.1080/13873954.2013.809364)

BibTex entry:

```
% This file was created with JabRef 2.6.  
% Encoding: Cp1252  
  
@ARTICLE{acinpaper,  
    author = {Speicher, Katrin and Steinboeck, Andreas and Wild, Daniel and Kiefer,  
              Thomas and Kugi, Andreas},  
    title = {An integrated thermal model of hot rolling},  
    journal = {Mathematical and Computer Modelling of Dynamical Systems},  
    year = {2014},  
    volume = {20},  
    pages = {66--86},  
    number = {1},  
    doi = {10.1080/13873954.2013.809364},  
    url = {http://www.tandfonline.com/doi/abs/10.1080/13873954.2013.809364}  
}
```

Link to original paper:

[http://dx.doi.org/10.1080/13873954.2013.809364](https://dx.doi.org/10.1080/13873954.2013.809364)
<http://www.tandfonline.com/doi/abs/10.1080/13873954.2013.809364>

Read more ACIN papers or get this document:

<http://www.acin.tuwien.ac.at/literature>

Contact:

Automation and Control Institute (ACIN)
Vienna University of Technology
Gusshausstrasse 27-29/E376
1040 Vienna, Austria

Internet: www.acin.tuwien.ac.at
E-mail: office@acin.tuwien.ac.at
Phone: +43 1 58801 37601
Fax: +43 1 58801 37699

Copyright notice:

This is the authors' version of a work that was accepted for publication in Mathematical and Computer Modelling of Dynamical Systems. Changes resulting from the publishing process, such as peer review, editing, corrections, structural formatting, and other quality control mechanisms may not be reflected in this document. Changes may have been made to this work since it was submitted for publication. A definitive version was subsequently published in K. Speicher, A. Steinboeck, D. Wild, T. Kiefer, and A. Kugi, "An integrated thermal model of hot rolling", *Mathematical and Computer Modelling of Dynamical Systems*, vol. 20, no. 1, pp. 66–86, 2014. doi: [10.1080/13873954.2013.809364](https://doi.org/10.1080/13873954.2013.809364)

RESEARCH ARTICLE

An integrated thermal model of hot rolling

Katrin Speicher^{a*}, Andreas Steinboeck^a, Daniel Wild^b, Thomas Kiefer^b, and Andreas Kugi^a

^a*Automation and Control Institute, Vienna University of Technology, Vienna, Austria;*

^b*AG der Dillinger Hüttenwerke, Dillingen, Germany*

(Received 00 Month 200x; final version received 00 Month 200x)

During the heavy plate rolling process, different production steps, i.e., roll passes, descaling passes, and air cooling periods, influence the temperature evolution of the plate. All these relevant aspects are covered by a one-dimensional thermal model proposed in this paper. Experiments were conducted in a rolling mill under realistic rolling conditions to parametrise and validate the model. Using pyrometer measurements, a simple model adaption strategy is developed, which can cope with uncertainties in the initial temperature profile. The model provides accurate predictions of the temperature evolution of the plate during the whole rolling process from the plate's exit of the furnace to the last pass. Thus, it can be used for scheduling the production process. Based on the model, an observer can be designed.

Keywords: temperature evolution, heat transfer, descaling, air cooling, heavy plate rolling

1. Introduction

To meet the high quality requirements of nowadays steel production, it is vital that the rolling takes place in the prescribed temperature range. Moreover, the temperature largely influences the yield stress and thus the rolling force and torque. Therefore, the temperature evolution of the plate has to be considered when planning the roll passes and scheduling the whole production process. In the following, the different production steps are outlined by means of an overview of the considered rolling mill shown in Figure 1 and their influence on the temperature evolution of the plate is briefly described.

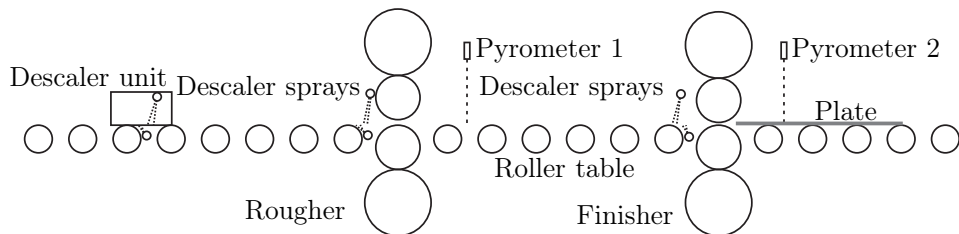


Figure 1. Outline of the considered rolling mill.

When the slab is reheated in a furnace up to 1450 K, primary scale grows on the surfaces of the slab, which has to be removed prior to the rolling process because it would otherwise affect the surface quality of the rolled plate. The scale is removed

*Corresponding author. Email: speicher@acin.tuwien.ac.at

by high pressure water jets in a dedicated descaler unit. The water jets expose the surfaces to a thermal shock and cause strong temperature gradients in the surface layers. In the next step, the plate is rolled in several passes to the desired width in the roughing mill and to the desired thickness in the finishing mill. During the roll passes, the plate cools down because of the contact with the work rolls. As they are much colder than the plate, the cooling effect is strong, but only confined to a thin surface layer due to the short contact time. The cooling effect is counteracted by reheating due to dissipated deformation energy and frictional heat generated at the contact surfaces to the work rolls. Between two passes, the plate is subjected to air cooling periods of predefined lengths. As the plate lies on the roller table, the cooling of the lower surface is retarded. During longer waiting periods, secondary scale may grow on the plate surfaces. To remove it, the roughing mill and the finishing mill are equipped with descaler sprays. These sprays can also be used for deliberate cooling of one of the surfaces, e.g., if a plate exhibits temperature-induced flatness defects. The plate is normally descaled at least before the first pass at the finishing mill. After the final roll pass, the plate is cooled down in the cooling section and finally leveled to reduce residual stresses and to improve the flatness (not shown in Fig. 1).

The model, which is presented in this paper, takes into account all production steps until the last pass in the finishing mill. This includes the passes themselves, the air cooling in the transport and waiting periods, and the temperature shocks caused by the descaler unit and the descaler sprays at the mill stands. Numerous measurements give evidence of the accuracy of the model. However, it is computationally inexpensive and thus suitable for real time applications. It can be used for observer and controller design as well as for scheduling and optimising the process. Similar models can be found in, e.g., [1–5]. The differences between the model proposed here and existing models are discussed in the course of the paper.

The paper is organised as follows: First, a general formulation of the heat conduction problem is given in Section 2.1. The heat conduction equation forms the common ground of all the submodels of the different production steps and only the boundary conditions and source terms change. The different boundary conditions are presented in Sections 2.2 to 2.4. Each of these sections also gives an overview of existing models in the literature. The identification of the model parameters based on measurements is presented in Section 3. In Section 4, the temperature evolution of the plate during the whole rolling process is simulated and compared to pyrometer measurements. Furthermore, a simple adaption strategy is proposed. Conclusions are drawn in Section 5.

2. Mathematical modelling

2.1. Heat conduction equation

To model the temperature evolution of the plate, the general heat conduction problem is formulated. As the temperature gradients in the thickness direction y of the plate are bigger than in its width and length, the heat conduction along the thickness direction dominates. Thus, we will consider the one-dimensional form of the heat conduction equation, i.e.,

$$\rho c_p \frac{\partial T(y, t)}{\partial t} = \frac{\partial}{\partial y} \left(\lambda \frac{\partial T(y, t)}{\partial y} \right) + \dot{Q}, \quad y \in (0, H), \quad t > 0 \quad (1)$$

with the initial conditions

$$T(y, 0) = T_0(y), \quad y \in [0, H] \quad (2)$$

and suitable boundary conditions. Here, $T(y, t)$ denotes the temperature field along the thickness direction and \dot{Q} refers to a heat source. The expression ρc_p , with the specific heat capacity c_p and the mass density ρ , as well as the thermal conductivity λ are regarded as temperature-dependent. They are shown in Figure 2 for a low-

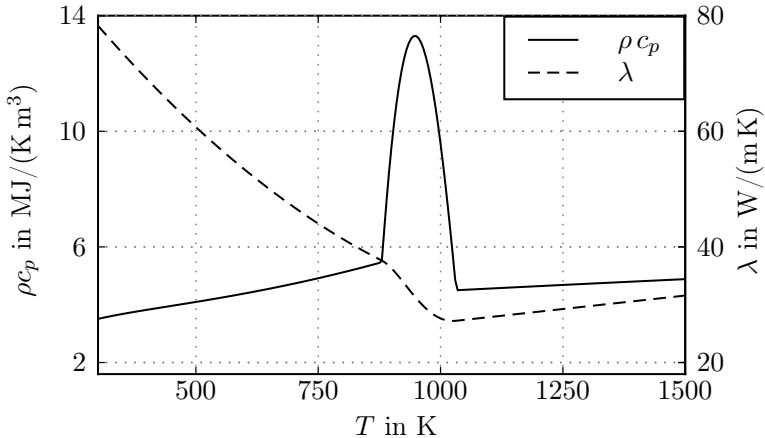


Figure 2. Temperature-dependent material parameters [6].

alloy steel. The striking peak of the heat capacity corresponds to a phase transition. These thermal characteristics depend on the steel grade and are calculated by means of polynomial approximations given in [6]. The boundary conditions supplementing (1) are formulated as Neumann boundary conditions, i.e., the heat fluxes out of the plate

$$\dot{q}_{lo} = -\dot{q}(0, t) = \lambda \frac{\partial T(y, t)}{\partial y} \Big|_{y=0} \quad (3a)$$

$$\dot{q}_{up} = \dot{q}(H, t) = -\lambda \frac{\partial T(y, t)}{\partial y} \Big|_{y=H} \quad (3b)$$

are prescribed. The positive heat fluxes \dot{q}_{lo} and \dot{q}_{up} are specified in the following sections.

The one-dimensional model in (1) to (3) is calculated at several points along the plate length yielding a temperature distribution in longitudinal direction. The boundary conditions for each of the thickness profiles are mostly the same, only the lengths of the air cooling periods between two passes vary depending on the length coordinate of the profile. As the considered mill is a reversing rolling mill, the tail end experiences a longer air cooling period than the head end before the first pass, but a shorter one before the second pass. Therefore, the differences balance out throughout the production process.

2.2. Air cooling

Air cooling is a recurrent transitional step in the production process of heavy plates. As air cooling periods can last up to 15 minutes and take place after each pass,

good understanding and precise modelling are crucial for the accuracy of the overall temperature model. A short overview of existing models is given in the following.

2.2.1. State of the art

During the air cooling periods, the plate loses heat by radiation and by convection. Usually both types of heat transfer are considered, see, e.g., [7], but as radiation is dominant at high temperatures, some other models capture only radiative heat transfer [2]. Cooling is usually assumed to be symmetrical at the bottom and the top side [1], although the situation is generally asymmetrical, see Figure 3. A model that accounts for re-radiation from the roller table is presented in [7]. Re-radiation is also considered in this paper because measurements indicate that the plate cools down asymmetrically.

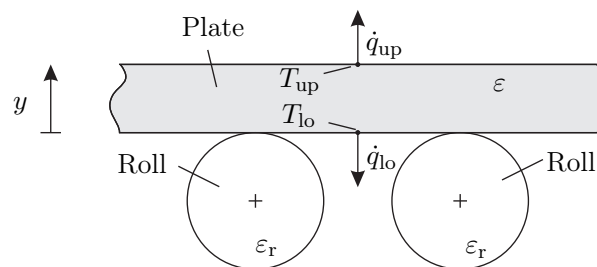


Figure 3. Plate on the roller table.

Radiative heat exchange is generally formulated using the Stefan–Boltzmann law, i.e., the heat flux is proportional to the fourth power of the surface temperature. The presence of scale hampers the radiative heat loss because the scale's low thermal conductivity leads to lower surface temperatures [7–10]. As a consequence, the radiative heat flux is reduced compared to the descaled case. Some authors, e.g., [7, 9–11], developed models to describe the scale formation and the heat conduction through the scale layer. However, in the considered rolling mill, the primary scale is removed right after the slab exits the furnace. Secondary scale is much thinner and thus influences the temperature evolution only in a minor way. Therefore, it is refrained from modelling the formation of scale in this paper.

Furthermore, the employed emissivities strongly influence the resulting radiative heat flux. However, the choice of the right emissivity is a controversial issue because the emissivity may significantly depend on the surface temperature, the steel grade, and the current surface conditions, cf. [12]. Nevertheless, it is often assumed to be constant, e.g., in [1, 4, 7, 13, 14]. In the presented model, two different emissivity values, which are both identified based on experimental data, see Section 3, are used for the scaled and the descaled case. The different emissivity of the scaled plate should capture the different emissivity of the scale and its isolating effect.

Concerning the convective part, forced or natural convection can be taken into account. Natural convection prevails at low speeds, but forced convection dominates when the plates move faster, see [4]. The heat transfer coefficients for forced convection depend on the current velocity of the plate, e.g., [5, 14–16], and can be calculated by the formulae given in [17] or [18]. In the current paper, only forced convection is taken into account incorporating the plate velocity.

2.2.2. Air cooling model

As discussed in the previous paragraph, the air cooling heat fluxes consist of a radiative part \dot{q}_{rad} and a convective part \dot{q}_{conv} , i. e.,

$$\dot{q}_k = \dot{q}_{\text{rad},k} + \dot{q}_{\text{conv},k}, \quad k \in \{\text{up,lo}\}. \quad (4)$$

The radiative heat flux leaving the upper surface is formulated using the Stefan–Boltzmann law

$$\dot{q}_{\text{rad,up}} = \sigma \varepsilon (T_{\text{up}}^4 - T_{\infty}^4) \quad (5)$$

with the surface temperature $T_{\text{up}} = T(H, t)$, the assumed mean temperature $T_{\infty} \approx 288 \text{ K}$ of the surroundings, the Stefan–Boltzmann constant $\sigma = 5.67 \times 10^{-8} \text{ W}/(\text{m}^2 \text{ K}^4)$, and the emissivity ε of the plate. The emissivity is assumed to be constant. As its dependency on the temperature is not quantitatively known, it is risky to incorporate it in the model. In Section 3, it will be shown that a constant value of the emissivity can model the radiation properties in the investigated temperature range with sufficient accuracy.

To allow for the re-radiation from the roller table (cf. Fig. 3), the net radiation method [19] is employed. It yields the heat flux leaving the lower surface in the form

$$\dot{q}_{\text{rad,lo}} = \sigma \mathbf{P}_1^T \begin{bmatrix} T_{\text{lo}}^4 \\ T_{\text{r}}^4 \\ T_{\infty}^4 \end{bmatrix} \quad (6)$$

with the surface temperature $T_{\text{lo}} = T(0, t)$ and the assumed mean temperature $T_{\text{r}} \approx 323 \text{ K}$ of the roller table. As the rolls may heat up during the contact with the hot plates, their mean temperature is assumed to be higher than the temperature of the surroundings. However, this temperature influences the temperature evolution of the plate only in a minor way. The vector \mathbf{P}_1^T is the first row of the matrix

$$\mathbf{P} = -\text{diag}(\boldsymbol{\varepsilon}) [\mathbf{I} - \mathbf{F}(\mathbf{I} - \text{diag}(\boldsymbol{\varepsilon}))]^{-1} \mathbf{F} \text{diag}(\boldsymbol{\varepsilon}) + \text{diag}(\boldsymbol{\varepsilon}). \quad (7)$$

which results from the net radiation method [19]. The emissivity vector $\boldsymbol{\varepsilon} = [\varepsilon \ \varepsilon_{\text{r}} \ \varepsilon_{\infty}]^T$ contains the emissivities of the plate, the roller table, and the surroundings. While ε and ε_{r} have to be identified based on experimental data, the emissivity of the surroundings is set to $\varepsilon_{\infty} = 1$. View factors, which are assembled in the view factor matrix \mathbf{F} , depend on the geometry of the roller table and are calculated by means of Hottel's crossed-string method [20, 21]. \mathbf{I} denotes the identity matrix.

The convective part of the heat flow \dot{q}_{conv} is calculated by

$$\dot{q}_{\text{conv},k} = h_{\text{conv},k} (T_k - T_{\infty}), \quad k \in \{\text{up,lo}\}, \quad (8)$$

with the mean convective heat transfer coefficient $h_{\text{conv},k}$, which is obtained by averaging the local convective heat transfer $h_{\text{conv},k,x}$ over the so-called characteristic length. For the upper surface, the characteristic length equals the plate length L . For the lower surface, it is the distance between two rolls. The local convective heat

transfer coefficient reads as

$$h_{\text{conv},k,x} = \frac{Nu_x \lambda_{\text{air}}}{x} \quad (9)$$

with the distance from the leading edge x of the plate, the local Nusselt number Nu_x , and the conductivity of the air λ_{air} . Different approaches for modelling the local Nusselt number for laminar or turbulent flow can be found in the literature, see [19, 22]. In the current paper, the approaches

$$Nu_{x,\text{lam}} = \frac{1}{\sqrt{\pi}} Re_x^{\frac{1}{2}} \frac{Pr^{\frac{1}{2}}}{(1 + 1.973 Pr^{0.272} + 21.29 Pr)^{\frac{1}{6}}}, \quad (10)$$

and

$$Nu_{x,\text{turb}} = 0.0296 Re_x^{\frac{4}{5}} Pr^{\frac{1}{3}} \quad (11)$$

for laminar and turbulent flow, respectively, are used. The Prandtl number

$$Pr = \frac{\nu_{\text{air}} \rho_{\text{air}} c_{p_{\text{air}}}}{\lambda_{\text{air}}} \quad (12)$$

and the local Reynolds number

$$Re_x = \frac{vx}{\nu_{\text{air}}} \quad (13)$$

depend on the material properties of the air, i.e., the density ρ_{air} , the specific heat capacity $c_{p_{\text{air}}}$, and the kinematic viscosity ν_{air} , as well as on the velocity v of the plate. Equation (10) is an approximate solution of the balances of energy and momentum. In the case of air, the error between the exact and the approximate solution is lower than 0.15% [19].

2.3. Descaling

Descaling is mainly a preparatory step for the rolling and aims at removing the scale from the surface. The sprays expose the surfaces to thermal shocks, which result in strong temperature gradients in the surface layer. Compared to air cooling the modelling of the descaling process includes a high degree of uncertainty. In the following, different approaches reported in the literature will be presented.

2.3.1. State of the art

Most published models are phenomenological models based on experimental data. As the experimental conditions differ significantly, the results are also very different, e.g., constant heat transfer coefficients in the range from 1162 W/(m² K) to 20 920 W/(m² K) are reported in [7] and [23], respectively. A dependence of the heat transfer coefficient on the impact pressure is suggested in [24], where different constant values from 2000 W/(m² K) to 8000 W/(m² K) are used for different levels of spray pressure. A linear relationship between the heat transfer coefficient and the impact pressure was experimentally found in [25] for a considered impact pressure range from 4.82 bar to 8.07 bar. An increase of the heat transfer coefficient with increasing pressure was also noted in experiments in [26].

Apart from the modelling approaches depending on the pressure, formulations

considering the volume flow as a relevant parameter were also proposed. Their relevance was experimentally demonstrated in [27]. According to [28], the heat transfer coefficient additionally depends on the surface temperature. In addition to the mass flow also the difference between the surface and the water temperature influences the heat transfer coefficient as it is reported in [8, 29]. In [4], the heat flux is modelled as a function of the volume flow and the water temperature.

More theoretical investigations that rely on the concept of boiling heat transfer, e.g., [30–32], or a combination of boiling, radiation, and convection through a steam layer were proposed in [1, 12, 33]. In these cases, the heat flux depends on quantities that are usually unknown, e.g., the amount of steam generated. Thus, the advantage of a sound physical interpretation is outweighed by the lack of precise data.

In summary, it can be stated that modelling the temperature evolution during descaling is a difficult task. There is no consensus about the factors influencing the heat transfer from the plate to the water of the descaler spray. The impact pressure and the volume flow are usually assumed to affect the heat transfer. But the modelling approaches of the heat transfer coefficient were derived under strongly different experimental conditions, which do not fit the normal production conditions in the considered rolling mill. Therefore, none of the descaling models found in the literature can be adopted as it is.

2.3.2. Descaling model

In the considered rolling mill, the descaler unit and the descaler sprays at both roughing and finishing mill use a central water supply. Therefore, the pressure is the same for all three devices, apart from some oscillations. The water volume flow mainly depends on the installed nozzles. Consequently, each spray header is characterized by a constant pressure and a constant volume flow. Therefore, the heat transfer during descaling can be modelled by a convective boundary condition

$$\dot{q}_k = h_{d,k} (T_k - T_w), \quad k \in \{\text{up,lo}\}, \quad d \in \{\text{DU, DR, DF}\}. \quad (14)$$

Here, T_w is the water temperature and $h_{d,k}$ is the heat transfer coefficient, which is generally different for the descaler unit (DU), the descaler sprays at the roughing mill (DR), and the descaler sprays at the finishing mill (DF). Moreover, $h_{d,k}$ may be different for the upper (up) and the lower (lo) spray header. The heat transfer coefficients will be identified based on experimental data in Section 3.

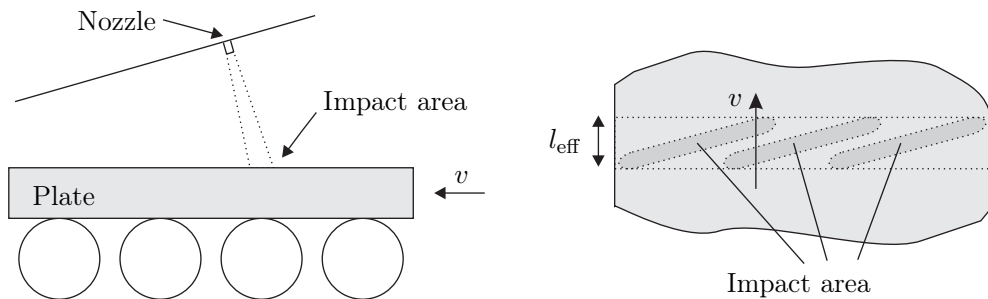


Figure 4. Impact of descaling spray: side view (left), top view (right).

This descaling boundary condition is used for an effective descaling time $t_{\text{eff}} = l_{\text{eff}}/v$ with the plate velocity v and the effective length of the impact area l_{eff} as indicated in Figure 4. The effective length l_{eff} depends on the spray geometry and the position of the nozzles. Important design parameters are the distance between

the nozzles and the surface of the plate as well as the fan angle and the rotational angle of the spray.

2.4. Heat transfer during the roll passes

During the roll passes, the temperature of the plate is influenced by three different mechanisms: heat loss towards the work rolls and heat generation because of deformation and friction. The plate loses heat at the contact interface with the cold work rolls. The work rolls heat up notably during that contact, but they are cooled down again by water sprays in the rest of the revolution. As a consequence, the surface of the work roll is cold again when it enters the roll gap the next time. Besides this cooling effect, the plate heats up because of dissipated deformation energy and frictional heat generated at the contact areas to the work rolls. Existing models of these temperature effects are summarised in the following.

2.4.1. State of the art

The heat generated by the deformation of the material is usually modelled as a volume heat source in the heat conduction equation. In [3, 5], additional deformation models are implemented to calculate the deformation energy. However, complicated deformation models are usually avoided and Pavlov's formula

$$Q = k_f \ln \left(\frac{H_{\text{in}}}{H_{\text{out}}} \right) \quad (15)$$

is used to determine the deformation energy [2, 12, 34]. H_{in} and H_{out} denote the entry and exit thickness of the roll pass, respectively, and k_f is the yield stress. Independent from the way of calculating the deformation energy, it is almost always assumed that only a certain fraction $\eta \in (0.85, 1)$ of the deformation energy is transformed into heat, see, e.g., [5, 35, 36]. In all these publications, the heat of deformation is distributed uniformly through the thickness of the plate. Although it is stated in [37] that the deformation heat generation is inhomogeneous just as the deformation itself, the assumption of uniform heat generation seems to be sufficiently accurate.

In contrast to the heat generated by deformation in the whole plate volume, friction and heat transfer at the plate-work roll contact are local phenomena. As the work roll temperature plays an important role in the contact problem, the roll volume is also modelled in most cases, e.g., in [1, 2, 14, 34, 35, 38]. Although the work rolls heat up significantly during the contact with the plate, the temperature variation is confined to a thin surface layer because the rolls are cooled down again by water sprays after the contact.

Published modelling approaches for the contact heat transfer differ considerably. In some cases, e.g., [4, 7, 23], the contact problem is solved analytically. However, the analytical solution can only be derived, if some assumptions are made, including that the plate and the work roll are two semi-infinite solids in perfect contact with homogeneous initial temperature profiles. Notwithstanding that this assumption may be untenable, the analytical solution of the contact problem is widely used. In contrast, most authors use a convective boundary condition to model the cooling due to the work rolls, e.g., [34, 35, 39]. The usually constant heat transfer coefficients range from $6 \text{ kW}/(\text{m}^2 \text{ K})$ in [24] to $45 \text{ kW}/(\text{m}^2 \text{ K})$ in [35]. In [34, 37, 40], it was experimentally found that the heat transfer coefficient can be non-uniform along the roll gap. It may also depend on the reduction ratio, the rolling speed, and the lubrication conditions [34, 37]. The effect of the pressure on the effective contact

area and the heat transfer coefficient is quantified in [40]. The derived pressure-dependent formula for the heat transfer coefficient also depends on the yield stress of the plate material, the surface roughness, and the conductivities of the plate and the work roll. The same relation was also used in [36, 41, 42]. However, this approach does not take into account the heat transfer in regions of the contact area where the plate and the roll material are not in direct contact, e.g., at oxidised sections, at lubricating films, at boiling water films, or in cavities created by the surface roughness. Some approaches considering heterogeneous interface conditions can be found in [43–46].

The effect of friction is usually modelled by a surface heat source, where the heat generation rate equals the product of the shear stress due to friction and the absolute velocity difference of the plate and the work roll in the contact surface [5, 35, 41, 47]. This velocity difference increases near the entry (backward slip) and the exit region (forward slip) of the roll gap, which causes higher heat fluxes in these regions. To model the shear stress due to friction, three different approaches are used: the Coulomb friction model [2, 3, 23, 24, 34], the Tresca friction model [36, 46], and the Wanheim-Bay friction model. They are compared in [48, 49]. The generated heat is sometimes equally distributed to the work roll and to the plate [5] or mainly allocated to the plate [4, 23].

There is no consensus in the literature about the relative importance of these three effects (deformation, heat loss to work rolls, friction) for the temperature evolution of the plate. Sometimes it is assumed that the conduction to the work rolls is the main heat loss during the production process. In [2], however, it is argued that the frictional heat compensates for the cooling effect of the work rolls. In contrast, in [35], the contribution of frictional heat to the temperature evolution is expected to be low. It can be concluded that the influence of the different effects on the plate temperature strongly depends on the production conditions and also on the properties of the plate itself. In the following, a model is presented that takes into account all three aspects.

2.4.2. Roll pass model

During the roll passes, the plate and the work roll are thermally coupled. Consequently, the heat conduction equation of the plate (cf. (1)) has to be solved simultaneously with the heat conduction equation of the work rolls. There, the heat flows mainly in radial direction, so that only the one-dimensional heat conduction equation in cylindrical coordinates is considered for the work rolls, i.e.,

$$\rho_{\text{wr},k} c_{p_{\text{wr},k}} \frac{\partial T_{\text{wr},k}(r_k, t)}{\partial t} = \frac{1}{r_k} \frac{\partial}{\partial r_k} \left(r_k \lambda_{\text{wr},k} \frac{\partial T_{\text{wr},k}(r_k, t)}{\partial r_k} \right), \quad (16)$$

$$r_k \in (R - \delta_r, R), \quad t > 0, \quad k \in \{\text{up,lo}\}$$

with the temperature $T_{\text{wr},k}(r_k, t)$ of the respective work roll and appropriate initial and boundary conditions. The solution of (16) is restricted to a boundary layer of thickness δ_r because the cyclic heating and cooling of the work roll during each revolution is confined to this small boundary layer. In simulation studies, it was found that $\delta_r = 20$ mm is a reasonable value for a work roll with a radius $R \approx 0.5$ m and rolling speeds higher than 2 m/s. Because of this small value for δ_r , the relative change of the radial coordinate r_k in the considered boundary layer is rather small. Therefore, the curvature of the boundary layer could be neglected, implying that (16) would reduce to a standard 1D heat conduction problem in Cartesian coordinates similar to (1).

The temperature-dependent material parameters $\rho_{\text{wr},k}$, $c_{p_{\text{wr},k}}(T_{\text{wr},k})$, and

$\lambda_{\text{wr},k}(T_{\text{wr},k})$ are assumed to be the same for both work rolls. Furthermore, the mean work roll radius $R = (R_{\text{wr},\text{lo}} + R_{\text{wr},\text{up}})/2$ is used for the calculations. As a consequence, the geometric situation shown in Figure 5 is symmetric and thus easier to handle. The absolute thickness reduction $\Delta H = H_{\text{in}} - H_{\text{out}}$ and the length $L_d = \sqrt{R\Delta H - \Delta H^2/4}$ of the contact arc are the same for both work rolls.

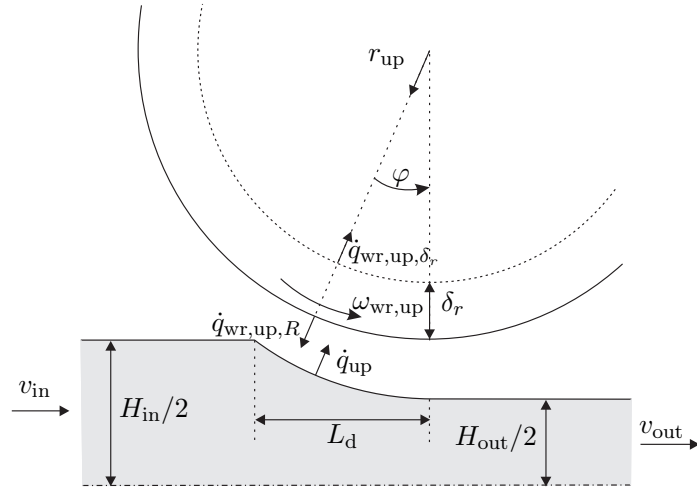


Figure 5. Geometry of the roll gap.

The boundary conditions of the plate are given by

$$\dot{q}_k = \dot{q}_{\text{cond},k} - \frac{1}{2}\dot{q}_{\text{fric},k}. \quad (17)$$

The heat fluxes $\dot{q}_{\text{wr},k,\delta_r}$ and $\dot{q}_{\text{wr},k,R}$ at the inner and the outer boundary of the work rolls, respectively, see Figure 5, are specified by

$$\dot{q}_{\text{wr},k,\delta_r} = 0, \quad (18a)$$

$$\dot{q}_{\text{wr},k,R} = -\dot{q}_{\text{cond},k} - \frac{1}{2}\dot{q}_{\text{fric},k}, \quad (18b)$$

with the heat flux due to conduction $\dot{q}_{\text{cond},k}$, $k \in \{\text{up},\text{lo}\}$, from the plate to the respective work roll. The frictional heat source term $\dot{q}_{\text{fric},k}$ is equally distributed to the plate and the work rolls. The work roll surface outside the roll gap is cooled by water sprays so that the roll nearly reaches its quasi steady-state temperature 323 K again at the beginning of the next contact. This value was roughly estimated based on measurements of the work roll surface temperature right after a typical rolling sequence. This estimation is precise enough because the temperature difference between the work roll and the plate at the beginning of the contact is high compared to the uncertainty of the work roll temperature. Hence, the estimation does not have a significant influence on the model accuracy in terms of the temperature evolution of the plate. Based on this estimation, it is not necessary to compute the whole temperature history of the work roll. It suffices to compute the contact heat transfer between the plate and the work roll and to reset the work roll temperature profile to its quasi steady-state temperature before the next contact.

The heat flux due to conduction is modelled in the form

$$\dot{q}_{\text{cond},k} = h_{\text{cond},k} (T_k - T_{\text{wr},k,R}), \quad k \in \{\text{up},\text{lo}\}, \quad (19)$$

with the surface temperatures of the work rolls $T_{\text{wr},k,R} = T_{\text{wr},k}(r_k = R, t), k \in \{\text{up,lo}\}$. The heat transfer coefficients are calculated as proposed in [40], i. e.,

$$h_{\text{cond},k} = \frac{\lambda_{\text{com},k}}{f_h} \left(\frac{F}{3WL_d k_f} \right)^{e_h}, \quad k \in \{\text{up,lo}\}, \quad (20)$$

with the yield stress k_f , the rolling force F , the plate width W and the combined thermal conductivity

$$\lambda_{\text{com},k} = \frac{\lambda(T_k)\lambda_{\text{wr},k}(T_{\text{wr},k,R})}{\lambda(T_k) + \lambda_{\text{wr},k}(T_{\text{wr},k,R})}. \quad (21)$$

The parameters e_h and f_h are identified based on experimental data, see Section 3.

To calculate the frictional heat flux $\dot{q}_{\text{fric},k}$ in (17) and (18b), the Coulomb friction model is adopted. The generated friction heat flux thus follows as

$$\dot{q}_{\text{fric},k} = \mu \frac{F}{WL_d} |v_{\text{rel},k}|, \quad k \in \{\text{up,lo}\}, \quad (22)$$

with the friction parameter μ which is also identified in Section 3. The local relative velocity $v_{\text{rel},k}$ is the difference between the circumferential speed $v_{\text{wr},k}$ of the work roll and the local tangential velocity $v_t(\varphi)$ of the plate surface and reads as

$$v_{\text{rel},k}(\varphi) = v_{\text{wr},k} - v_t(\varphi) = R\omega_{\text{wr},k} - \frac{v_{\text{out}}H_{\text{out}}}{\cos(\varphi)(H_{\text{out}} + 2R(1 - \cos(\varphi)))}. \quad (23)$$

The local plate velocity is calculated via the continuity equation under the assumption of the slab model.

It remains to model the heat of deformation. As the overall model should be suitable for real-time application, the calculation of the exact deformation field is omitted. Instead, Pavlov's equation (15) is used to calculate the deformation energy. It is assumed that $\eta = 90\%$ of the deformation energy is transformed into heat.

2.5. Discretisation

The heat conduction problem is discretized by means of the finite difference method [50, 51]. For the discretisation of the spatial partial derivatives, central difference quotients are used. The backward Euler method is utilised to discretise the time derivative, leading to an implicit formulation of the model in the form, i. e.,

$$\mathbf{f}(\mathbf{x}_{j+1}, \mathbf{x}_j, \mathbf{u}_{j+1}) = \mathbf{0}. \quad (24)$$

The state vector $\mathbf{x}_j = \mathbf{x}(t_j)$ normally contains the temperatures at the grid points of the plate at the time t_j . For the roll pass model, it has to be extended by the temperatures at the grid points of the two work rolls. The input vector $\mathbf{u}_j = \mathbf{u}(t_j)$ depends on the considered boundary conditions as well as on the heat source term. As the boundary conditions change depending on the production step, the system (24) is switched. The system (24) is non-linear because the boundary conditions of the air cooling model contain the fourth power of the surface temperatures, cf. (5) and (6). To circumvent this non-linearity when solving (24), the boundary conditions are linearised at the respective operating point (surface temperatures of the previous time step).

3. Parameter identification

To identify the unknown parameters $\varepsilon, \varepsilon_r, e_h, f_h, \mu$, and $h_{d,k}, k \in \{\text{up,lo}\}, d \in \{\text{DU,DR,DF}\}$, experiments were carried out in an industrial rolling mill of the AG der Dillinger Hüttenwerke. In the following, these experiments and the parameter identification are briefly described.

3.1. Experimental set-up

Two different types of experiments were conducted:

- (a) experiments with a test plate instrumented with thermocouples to investigate the temperature evolution during air cooling and descaling and
- (b) additional pyrometer measurements during normal production conditions to analyse the thermal effects of the roll passes.

In Table 1, the unknown model parameters are summarised and assigned to the experiment, in which they were identified.

Table 1. Unknown model parameters.

Parameter	Used in submodel	Equation	Identified in experiment
Emissivity ε of the plate	Air cooling	(5),(6)	a
Emissivity ε_r of the roller table	Air cooling	(6)	a
Descaling heat transfer coefficient $h_{d,k}$	Descaling	(14)	a
Exponent e_h	Roll pass	(20)	b
Factor f_h	Roll pass	(20)	b
Friction coefficient μ	Roll pass	(22)	b

3.1.1. Thermocouple measurements

A 380 mm thick plate was equipped with ten thermocouples placed at thickness coordinates $y_{\text{meas}} \in \{3, 5, 20, 140, 240, 360, 375 \text{ and } 377 \text{ mm}\}$. At 3 mm and 377 mm, two thermocouples were incorporated for redundancy reasons. After the plate was heated up in a furnace, it passed the descaling nozzles of the rolling mill several times.

Despite the absence of actual deformations (they would have damaged the thermocouples), the experiment was designed to be as similar as possible to the normal production procedure. Therefore, the descaling passes were performed in the specific temperature range at each device (descaler unit, roughing mill, finishing mill). At the roughing mill, two consecutive descaling passes were followed by an air cooling period, while an air cooling period was inserted after each pass in the descaler unit or at the finishing mill. At the mill stands, different typical speeds of the plate and different distances between the plate and the nozzles were investigated. Recall that the speed v directly influences the effective descaling time t_{eff} ; the height of the nozzles affects the effective descaling length l_{eff} and thus also the descaling time. During the intermediate air cooling periods, the strong temperature gradients caused by the thermal shock due to descaling balanced out so that the temperature profile at the beginning of the next descaling pass was similar to normal production conditions. As a consequence, the measurements during each descaling pass can be used to identify the heat transfer coefficient of the respective descaling sprays or to validate the identification. Furthermore, the measurements recorded during the air cooling periods can be used to identify the unknown emissivities.

3.1.2. Pyrometer measurements

Measurements of the heat transfer or the temperature during roll passes by means of thermocouples are hardly feasible because the thermocouples would be damaged by plastic deformations. Therefore, the surface temperatures of the plate were measured several times between two roll passes by pyrometers. The temperature evolution during the roll pass itself cannot be measured, but the warming of the boundary layer as a result of heat conduction after the cooling due to the contact with the cold work rolls can be captured by the pyrometers. The pyrometer measurements were performed after the identification of the unknown parameters of the air cooling model and the descaling model, i.e., only the roll pass model was not parametrised at this time. Therefore, the unknown parameters of the roll pass model could be identified based on the pyrometer measurements, although the temperature evolution due to a combination of air cooling periods, descaling passes and roll passes was measured by the pyrometers. Instead of a single pass, the whole production process and thus around 50 pyrometer measurements are used for the identification. The temperature of the upper surface is measured by 11 pyrometers positioned along the roller table, while only one pyrometer close to the finishing mill captures the temperature of the lower surface. The scarcity of bottom-side measurements is caused by the more difficult measurement conditions between the rolls of the roller table. The strategy of considering the whole production process is advantageous because then the uncertainty of the pyrometer readings has less influence on the identified parameters. Furthermore, the initial temperature profile at the furnace exit is given with high accuracy [52, 53], while the temperature is unknown at the beginning of any roll pass.

The pyrometer readings have to be preprocessed before they can be used for the parameter identification. As the head and the tail end of a plate are colder than its central part, only the measurements which can be attributed to the central fifth of the plate are considered. These measurements are averaged and the resulting mean value $\Theta(t_{\text{meas}})$ is regarded as the measured value.

3.2. Identification

3.2.1. Parameters of the air cooling and the descaling model

For the thermocouple experiment, the cost function

$$J = \sqrt{\frac{1}{t_e - t_s} \int_{t_s}^{t_e} \sum_{n=1}^{10} (T(y_{\text{meas},n}, t) - \Theta(y_{\text{meas},n}, t))^2 dt} \quad (25)$$

is formulated, which contains the quadratic error between the calculated temperatures $T(y_{\text{meas},n}, t)$ at the measuring points $y_{\text{meas},n}, n \in \{1, \dots, 10\}$, and the respective measured temperatures $\Theta(y_{\text{meas},n}, t)$. To identify the emissivities, an air cooling period from $t_s = t_{\text{air},s}$ to $t_e = t_{\text{air},e}$ is considered. For this air cooling period, the cost function (25) is minimized with respect to the emissivities of the plate ε and of the roller table ε_r , i.e., $\min_{\varepsilon, \varepsilon_r} J$. The minimization problem is solved in Matlab® using an interior-point algorithm. The identified parameters for the descaled plate are

$$\varepsilon = 1 \text{ and } \varepsilon_r = 0.53. \quad (26)$$

For physical reasons, the emissivity has to take a value between 0 (perfect mirror) and 1 (perfect emitter). The coincidence of the identified emissivity with its upper physical bound is remarkable because descaled metal surfaces normally have lower emissivities as they are more reflective. A further increase of the emissivity beyond the physical constraints would lead to a larger cost function so that $\varepsilon = 1$ is indeed the optimal parameter.

To identify the emissivity of the scaled plate, the air cooling period before the first descaling pass has to be considered. However, in the experiment (a) described in Section 3.1.1, this air cooling period lasted only for 55 s. Therefore, a similar experiment, where the air cooling period of the scaled plate was considerably longer, was used. The minimization problem is again solved with respect to both emissivities and yields the optimal parameters

$$\varepsilon = 0.65 \text{ and } \varepsilon_r = 0.51. \quad (27)$$

The identified emissivity ε of the plate is considerably lower than in the descaled case. Recall that the lower value may not only be attributed to the different radiative properties of the scale layer but also reflects its isolating effect. The emissivity ε_r of the roller table obtained in the first identification is confirmed by the second identification, although the experiment took place on a different part of the roller table. As a consequence, only a single value can be used in the air cooling model.

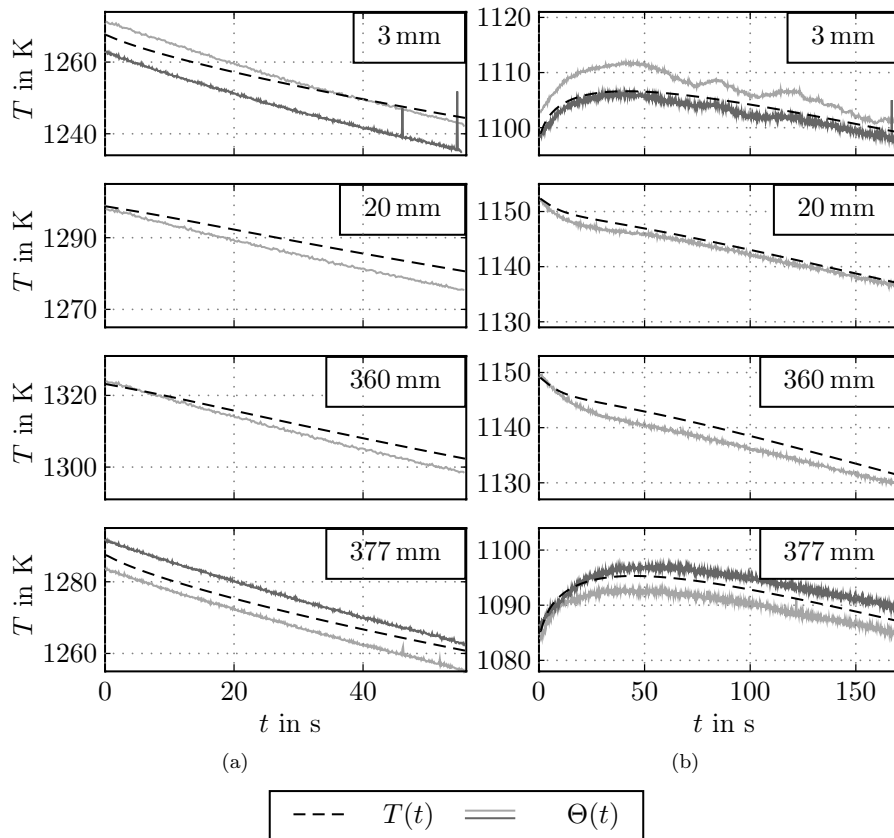


Figure 6. Comparison of measured (solid lines) and simulated temperatures (dashed lines) during air cooling periods: (a) scaled plate (not used for identification) (b) descaled plate (used for identification).

In Figure 6, a comparison of the measured temperatures (solid lines) and the

simulated temperatures (dashed lines) using the optimized emissivities is shown for the thermocouples at 3 mm, 20 mm, 360 mm and 377 mm. As two thermocouples were incorporated at 3 mm and at 377 mm for redundancy reasons, the respective subfigures contain two measured temperatures instead of one. In Figure 6 as well as in the following ones, the time scale was shifted to 0. While the plate continuously cools down in Figure 6(a), the measured temperatures at the outermost thermocouples rise at the beginning of the air cooling period in Figure 6(b). This temperature rise is caused by heat conduction after the thermal shock due to the descaler sprays. As the air cooling period of the scaled plate in Figure 6(a) takes place before the first descaling pass, no similar temperature rise can be observed. The good agreement of simulation and measurement data is also achieved for other air cooling periods and for the other thermocouples whose measurements are not presented in Figure 6. No pronounced dependency of the emissivity on the temperature could be identified in the different air cooling periods. However, the surface temperatures ranged only from about 1000 K to 1150 K in the experiments. For this limited temperature range, the simplifying assumption of a constant emissivity is sufficiently accurate.

The descaling heat transfer coefficients (cf. (14)) are identified by analysing the descaling process together with the subsequent air cooling period. This is because the descaling pass itself lasts only for about 20 ms and the associated fast temperature changes cannot be accurately tracked by the thermocouples (sampling period 200 ms). During the air cooling period, the combined warming of the boundary layer and cooling of the core of the plate due to heat conduction is adequately captured by measurements. Therefore, the cost function (25) is considered for periods ranging from $t_s = 0$ to $t_e = t_{desc,d}$, $d \in \{DU, DR, DF\}$, which consist of a descaling pass ($t = 0$) and the subsequent air cooling period. The resulting optimized descaling heat transfer coefficients are summarised in Table 2. The differences between the heat transfer coefficients for the upper and the lower surfaces at each device can be explained by higher impact pressure or higher volume flow.

Table 2. Identified descaling heat transfer coefficients (in W/(m² K)).

$h_{DU,lo}$	$h_{DU,up}$	$h_{DR,lo}$	$h_{DR,up}$	$h_{DF,lo}$	$h_{DF,up}$
7×10^6	3×10^6	8×10^4	9×10^4	3.56×10^4	4.22×10^4

In Figure 7, the measured temperatures (solid lines) are compared with the simulated temperatures (dashed lines) using the identified descaling heat transfer coefficients. For the descaler unit, measurements of a descaling pass, which was not used for identification, are shown in Figure 7(a). By contrast, the first 20 s of the measurements of the first descaling pass at the roughing mill, see Figure 7(b), were used for identification.

Several experiments were conducted to study the influence of the plate speed and the vertical distance between the upper spray header and the plate on the descaling heat transfer. Good agreement between simulation results based on the parameters from Table 2 and measurement data was observed for all experiments. The results for the thermocouple positions $y_{meas} \in \{5, 140, 240 \text{ and } 375 \text{ mm}\}$ (not shown in Figure 7) deviate in the same range. Thus, the assumption of a constant heat transfer coefficient for each spray header is justified. However, the heat transfer coefficients may not be valid for other rolling mills because they were identified for the specific descaler sprays in the considered rolling mill and generally depend on the considered operating conditions.

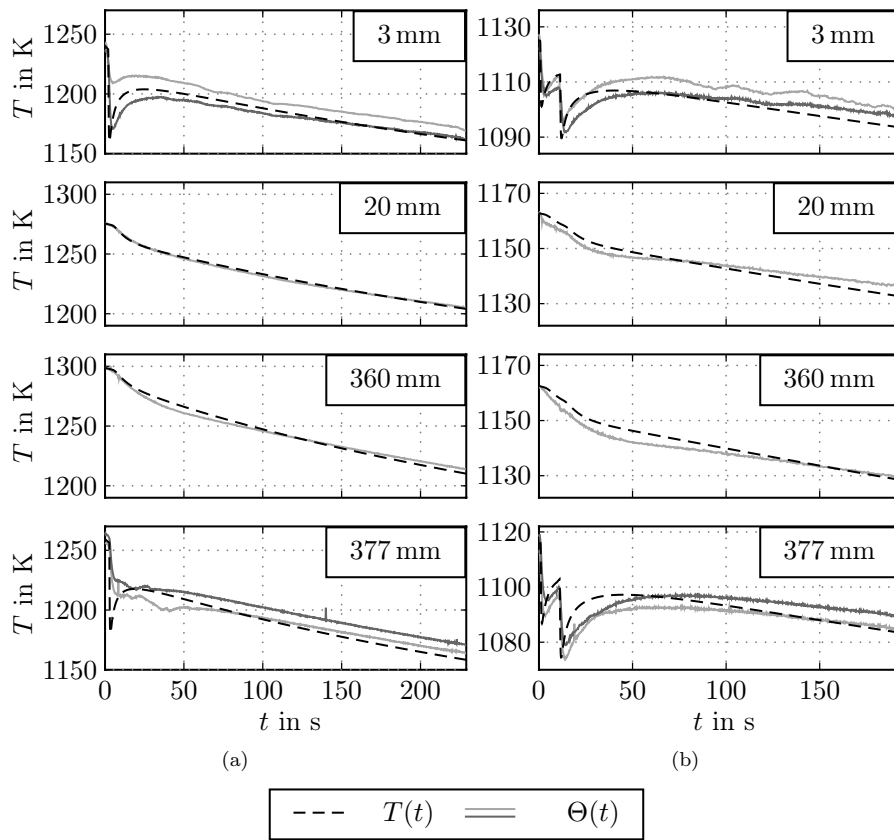


Figure 7. Comparison of measured (solid lines) and simulated temperatures (dashed lines) during a descaling pass: (a) descaler unit (not used for identification) (b) roughing mill (first 20 s were used for identification).

3.2.2. Parameters of the roll pass model

In contrast to the continuous measurements of the test plate with thermocouples, pyrometer readings are only available for times when the plate passes the fixed pyrometers. Therefore, the cost function is modified to

$$J = \frac{1}{\sqrt{N_{\text{up}} + N_{\text{lo}}}} \left(\sum_{n_{\text{up}}=1}^{N_{\text{up}}} (T_{\text{up}}(t_{\text{meas}, n_{\text{up}}}) - \Theta_{\text{up}}(t_{\text{meas}, n_{\text{up}}}))^2 + \sum_{n_{\text{lo}}=1}^{N_{\text{lo}}} (T_{\text{lo}}(t_{\text{meas}, n_{\text{lo}}}) - \Theta_{\text{lo}}(t_{\text{meas}, n_{\text{lo}}}))^2 \right)^{\frac{1}{2}} \quad (28)$$

for N_{up} and N_{lo} measurements of the upper and the lower surface temperature, respectively. This cost function (28) is minimized with respect to the unknown parameters of the roll pass model (the friction coefficient μ and the parameters e_h and f_h according to (20)), i.e., $\min_{\mu, e_h, f_h} J$. The resulting optimal parameters are given in Table 3. The parameters f_h and e_h are in the same range as those found in [40]. Note that the friction coefficient was also estimated by parameter identification, although it is a physical parameter with significant importance. However, the obtained value is physically meaningful and corresponds to the friction coefficients found in the literature, e.g., in [11, 34, 43].

Table 3. Optimal parameters of the roll pass model.

μ	f_h in μm	e_h
0.41	59.63	1.72

Figure 8 displays the results of the open loop simulation for plate 1, which was not used for identification. The evolution of the core temperature T_{core} and the surfaces temperatures T_{up} and T_{lo} as well as the corresponding pyrometer measurements are shown in Figure 8(a). The recurring drops of the surface temperatures are caused either by the contact of the plate with the work rolls or by descaling passes. After the thermal shock, the surface temperatures recover fast. As the minimum temperature at the end of the temperature drop is not significant, the temperature range in Figures 8(a), 9(a) and 10(a) is restricted to relevant temperature ranges. The error between the measured and the simulated surface temperatures is in the range from -20 K to 20 K , see Figure 8(b), which corresponds to less than $\pm 2\%$ of the actual temperature. Considering the usual measurement uncertainty of pyrometers used in this temperature range and that the measurements may be disturbed by water, steam, or scale, the achieved accuracy is satisfactory.

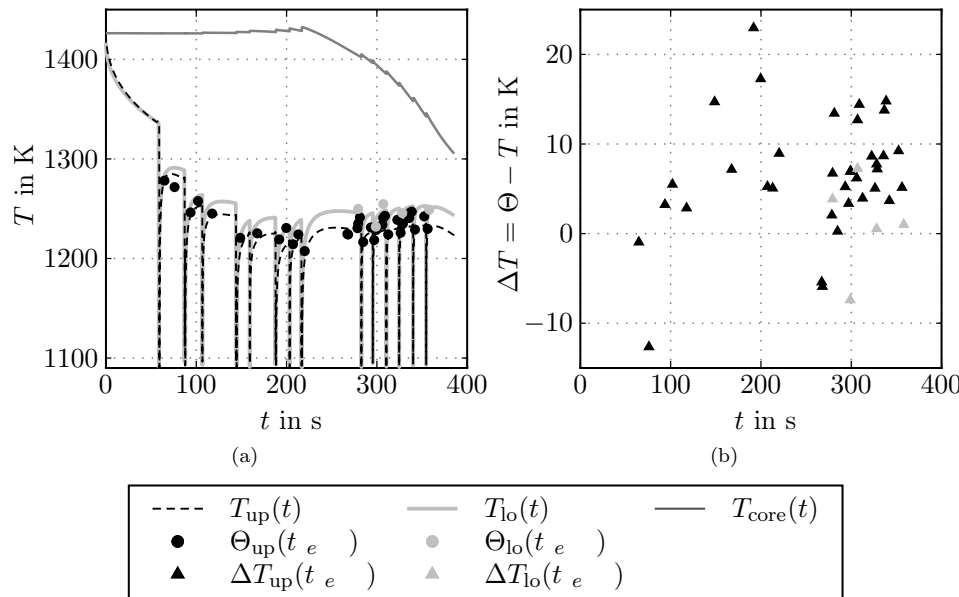


Figure 8. Comparison of the model with pyrometer measurements (plate 1): (a) temperature evolution (b) error.

4. Combined thermal model

The submodels described in Section 2 with the parameters identified in Section 3 are combined to the overall model so that the plate temperature can be calculated for the whole rolling process. As already indicated by Figure 8, the calculated and the measured temperatures agree well for simulated plate 1. In contrast, for plate 2, the simulated temperatures are about 20 K to 30 K too high compared to the pyrometer measurements, see Figure 9. This persistent deviation from the measurements may be attributed to an error in the initial temperature profile.

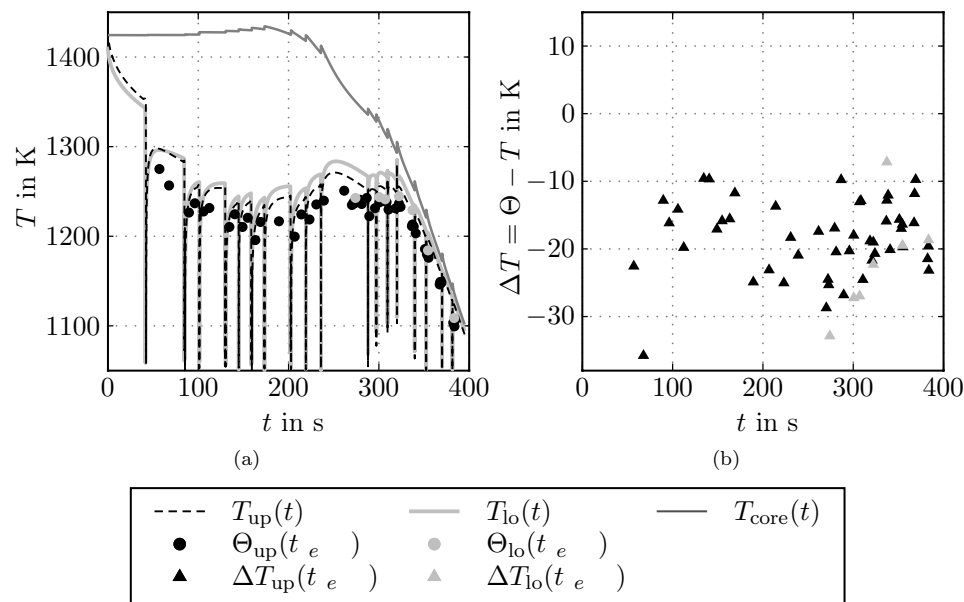


Figure 9. Comparison of the model with pyrometer measurements (plate 2): (a) temperature evolution (b) error.

Therefore, a simple adaption strategy is proposed in the following. The first pyrometer measurement $\Theta_{up}(t_{meas,1})$ after the first roll pass (pyrometer 1 in Figure 1) is used to correct the temperature profile by adding the error $\Delta T_{up} = \Theta_{up}(t_{meas,1}) - T_{up}(t_{meas,1})$ to the whole profile, i. e.,

$$\tilde{T}(y, t_{meas,1}) = T(y, t_{meas,1}) + \Delta T_{up}. \quad (29)$$

Using the adapted temperature $\tilde{T}(y, t_{meas,1})$ as new initial temperature, the process is simulated without further adaption, until the pyrometer 2 (see Figure 1) measures for the first time. Then, the temperature is again adjusted using the measured temperature $\Theta_{up}(t_{meas,2})$ in the same way as in (29). With this simple adaption strategy, a good agreement of simulation and measurement data is achieved as can be seen in Figure 10.

5. Conclusions and outlook

A thermal model was presented which covers the most significant influences on the temperature evolution of heavy plates during rolling. Using the proposed integrated model, the complete temperature evolution of a plate from the furnace exit to the last roll pass can be computed and predicted. To parametrise the model, different experiments were conducted. Therefore, a special instrumented test slab was developed and built. Based on the obtained measurements, the descaling heat transfer coefficients and the emissivities of the plate and of the roller table were identified. The roll pass model was parametrised using additional pyrometer measurements.

The resulting overall thermal model shows good agreement with thermocouple and pyrometer measurements. Compared to the pyrometer measurements, the model mismatch is smaller than $\pm 2\%$ of the actual surface temperature in Kelvin. However, the real power of the model can be deployed by exploiting the pyrometer readings. The simple adaption strategy proposed in the paper improves the tem-

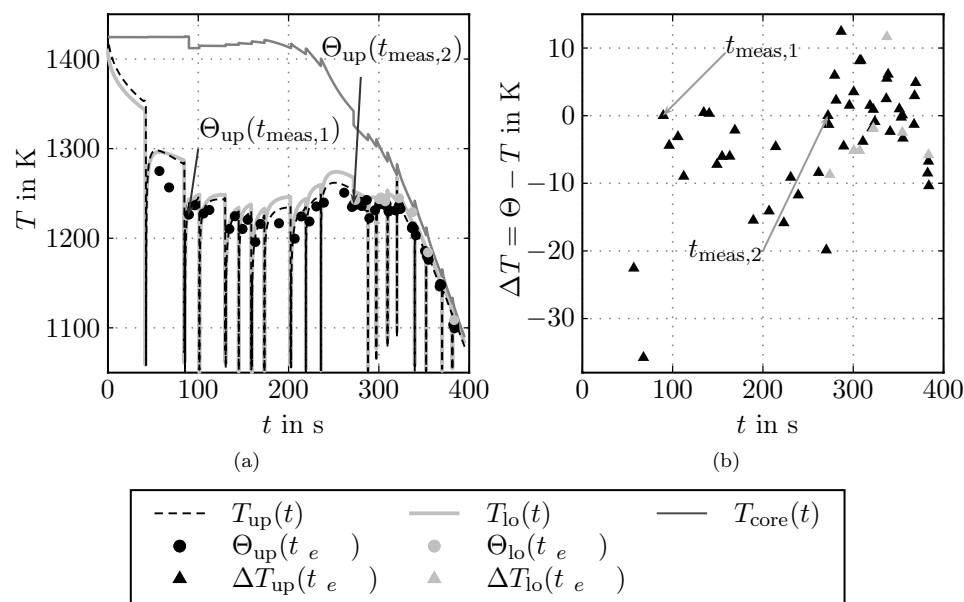


Figure 10. Comparison of the adapted model with pyrometer measurements (plate 2): (a) temperature evolution (b) error.

perature tracking capabilities of the model. A more sophisticated observer would lead to even higher accuracy.

The proposed model can be used to schedule and optimise the production process. Furthermore, an observer can be designed based on this model to improve the prediction of the temperature evolution of the plate. Additionally, the observer may be used to estimate the emissivity of the plate and hence to allow for the variability of the emissivity depending on the temperature and the steel grade. As the temperature influences the rolling process in multiple ways — roll force and torque, yield stress, microstructure — better knowledge of the temperature may lead to improved quality of the final product.

Acknowledgements

The authors from Vienna University of Technology highly appreciate the technical and financial support provided by AG der Dillinger Hüttenwerke. The second author highly appreciates financial support provided by the Austrian Academy of Sciences in the form of an APART-fellowship at the Automation and Control Institute of Vienna University of Technology.

References

- [1] R. Colas, *Modelling heat transfer during hot rolling of steel strip*, Modelling and Simulation in Materials Science and Engineering 3 (1995), pp. 437–453.
 - [2] C. Devadas and I. Samarasekera, *Heat transfer during hot rolling of steel strip*, Ironmaking and Steelmaking 13 (1986), pp. 311–321.
 - [3] D. Jin, V. Hernandez-Avila, I. Samarasekera, and J. Brimacombe, *An integrated process model for the hot rolling of plain carbon steel*, Proceedings of the 2nd International Conference on Modelling of Metal Rolling Processes (1996), pp. 36–58.
 - [4] K. Yanagi, *Prediction of strip temperature for hot strip mills*, Transactions of the Iron and Steel Institute of Japan 16 (1976), pp. 11–19.

- [5] S. Zhou, *An integrated model for hot rolling of steel strips*, Journal of Materials Processing Technology 134 (2003), pp. 338–351.
- [6] K. Harste, *Untersuchung zur Schrumpfung und zur Entstehung von mechanischen Spannungen während der Erstarrung und nachfolgender Abkühlung zylindrischer Blöcke aus Fe-C Legierungen*, PhD dissertation, Technische Universität Clausthal, 1989.
- [7] F. Hollander, *A model to calculate the complete temperature distribution in steel during hot rolling*, Journal of the Iron and Steel Institute 208 (1970), pp. 46–74.
- [8] R. Viscorova, *Untersuchung des Wärmeübergangs bei der Spritzwasserkühlung unter Berücksichtigung des Einflusses der Verzunderung*, PhD dissertation, Technische Universität Clausthal, 2007.
- [9] R. Wendelstorff, K.H. Spitzer, and J. Wendelstorff, *Effect of oxide layers on spray water cooling heat transfer at high surface temperatures*, International Journal of Heat and Mass Transfer 51 (2008), pp. 4892–4901.
- [10] M. Torres and R. Colás, *A model for heat conduction through the oxide layer of steel during hot rolling*, Journal of Materials Processing Technology 105 (2000), pp. 258–263.
- [11] W. Chen, I. Samarasekera, A. Kumar, and E. Hawbolt, *Mathematical modelling of heat flow and deformation during rough rolling*, Ironmaking and Steelmaking 20 (1993), pp. 113–125.
- [12] F. Seredynski, *Prediction of plate cooling during rolling-mill operation*, Journal of the Iron and Steel Institute 211 (1973), pp. 197–203.
- [13] J. Spännar and P. Wide, *Finding a representative emissivity value by using grey box technique*, Proceedings of the 20th IEEE Instrumentation and Measurement Technology Conference IMTC 1 (2003), pp. 350–354.
- [14] M.P. Phaniraj, B.B. Behera, and A.K. Lahiri, *Thermo-mechanical modeling of two phase rolling and microstructure evolution in the hot strip mill: Part I. Prediction of rolling loads and finish rolling temperature*, Journal of Materials Processing Technology 170 (2005), pp. 323–335.
- [15] R.M. Guo, *Heat transfer of laminar flow cooling during strip acceleration on hot strip mill runout tables*, Iron and Steelmaker 20 (1993), pp. 49–59.
- [16] J.A. Visser and E.H. Mathews, *Numerical modelling of the heat transfer in and around a steel bar during hot rolling*, Communications in Applied Numerical Methods 4 (1988), pp. 657–664.
- [17] A. Hensel, P. Poluchin, and W. Poluchin *Technologie der Metallumformung: Eisen- und Nichteisenmetalle*, Vol. 1, Wiley-VCH, 1990.
- [18] J. Holman *Heat transfer*, 5 McGraw-Hill, 1981.
- [19] H.D. Baehr and K. Stephan *Heat and mass transfer*, 2 Springer, 2006.
- [20] H.C. Hottel, 1954, Heat transmission. in *Radiant heat transmission* McGraw-Hill.
- [21] R. Siegel and J.R. Howell *Thermal radiation heat transfer*, 4 Taylor and Francis, 2002.
- [22] J.H. Lienhard IV and J.H. Lienhard V *A heat transfer textbook*, 3 Phlogiston Press, 2008.
- [23] N. Hatta, J. Kokado, H. Nishimura, and K. Nishimura, *Analysis of slab temperature change and rolling mill line length in quasi continuous hot strip mill equipped with two roughing mills and six finishing mills*, Transactions of the Iron and Steel Institute of Japan 21 (1981), pp. 270–277.
- [24] F. Wang, L. Ning, Q. Zhu, J. Lin, and T. Dean, *An investigation of descaling spray on microstructural evolution in hot rolling*, The International Journal of Advanced Manufacturing Technology 38 (2008), pp. 38–47.
- [25] J.W. Choi and J.W. Choi, *Convective heat transfer coefficient for high pressure water jet*, Journal of the Iron and Steel Institute of Japan 42 (2002), pp. 283–289.
- [26] M. Raudenský and J. Horský, *Experimental study of thermal processes in hydraulic descaling*, Proceedings of the 3rd International Conference on Hydraulic Descaling (2000).
- [27] L. Bendig, M. Raudenský, and J. Horský, *Descaling with high pressure nozzles*, Proceedings of the 17th International Conference on Liquid Atomization and Spray Systems ILASS 17 (2001), pp. 781–786.
- [28] K. Sasaki, Y. Sugitani, and M. Kawasaki, *Heat transfer in spray cooling on hot surface*, Tetsu-to-Hagane (Journal of the Iron and Steel Institute of Japan) 65 (1979), pp. 90–96.
- [29] R. Viscorova, R. Scholz, K. Spitzer, and J. Wendelstorff, *Measurements of spray water cooling heat transfer coefficients under oxide scale formation conditions*, Proceedings of the Iron & Steel Technology Conference AISTech 2 (2006), pp. 519–528.
- [30] I. Pioro, W. Rohsenow, and S. Doerffer, *Nucleate pool-boiling heat transfer I: Review of parametric effects of boiling surface*, International Journal of Heat and Mass Transfer 47 (2004), pp. 5033–5044.
- [31] H. Robidou, H. Auracher, P. Gardin, and M. Lebouché, *Controlled cooling of a hot plate with a water jet*, Experimental Thermal and Fluid Science 26 (2002), pp. 123–129.
- [32] D. Wolf, F. Incropera, and R. Viskanta, *Local jet impingement boiling heat transfer*, International Journal of Heat and Mass Transfer 39 (1996), pp. 1395–1406.
- [33] Z.H. Liu and J. Wang, *Study on film boiling heat transfer for water jet impinging on high temperature flat plate*, International Journal of Heat and Mass Transfer 44 (2001), pp. 2475–2481.
- [34] C. Devadas, I. Samarasekera, and E. Hawbolt, *The thermal and metallurgical state of steel strip during hot rolling: Part I. Characterization of heat transfer*, Metallurgical and Materials Transactions A 22 (1991), pp. 307–319.
- [35] S. Serajzadeh, A.K. Taheri, and F. Mucciardi, *Prediction of temperature distribution in the hot rolling of slabs*, Modelling and Simulation in Materials Science and Engineering 10 (2002), pp. 185–203.
- [36] S. Serajzadeh and F. Mucciardi, *Modelling the work-roll temperature variation at unsteady state condition*, Modelling and Simulation in Materials Science and Engineering 11 (2003), pp. 179–194.
- [37] W. Chen, I. Samarasekera, and E. Hawbolt, *Fundamental phenomena governing heat transfer during rolling*, Metallurgical and Materials Transactions A 24 (1993), pp. 1307–1320.
- [38] A. Laasraoui and J.J. Jonas, *Prediction of temperature distribution, flow stress and microstructure during the multipass hot rolling of steel plate and strip*, Journal of the Iron and Steel Institute of Japan 31 (1991), pp. 95–105.
- [39] X. Duan and T. Sheppard, *Prediction of temperature evolution by FEM during multi-pass hot flat rolling of aluminium alloys*, Modelling and Simulation in Materials Science and Engineering 9 (2001), pp. 525–538.

- [40] C. Hlady, J. Brimacombe, I. Samarasekera, and E. Hawbolt, *Heat transfer in the hot rolling of metals*, Metallurgical and Materials Transactions B 26 (1995), pp. 1019–1027.
- [41] S. Serajzadeh, H. Mirbagheri, and A.K. Taheri, *Modelling the temperature distribution and microstructural changes during hot rod rolling of a low carbon steel*, Journal of Materials Processing Technology 125-126 (2002), pp. 89–96.
- [42] C.G. Sun and S.M. Hwang, *Prediction of roll thermal profile in hot strip rolling by the finite element method*, Journal of the Iron and Steel Institute of Japan 40 (2000), pp. 794–801.
- [43] S. Das, E. Palmiere, and I. Howard, *The cut-groove technique to infer interfacial effects during hot rolling*, Metallurgical and Materials Transactions A 35 (2004), pp. 1087–1095.
- [44] S. Das, I.C. Howard, and E.J. Palmiere, *A probabilistic approach to model interfacial phenomena during hot flat rolling of steels*, Journal of the Iron and Steel Institute of Japan 46 (2006), pp. 560–566.
- [45] Y.H. Li, M. Krzyzanowski, J.H. Beynon, and C.M. Sellars, *Physical simulation of interfacial conditions in hot forming of steels*, Acta Metallurgica Sinica 13 (2000), pp. 359–368.
- [46] S. Wang and A. Tseng, *Macro- and micro-modelling of hot rolling of steel coupled by a micro-constitutive relationship*, Materials & Design 16 (1995), pp. 315–336.
- [47] Z.C. Lin and C.C. Chen, *Three-dimensional heat-transfer and thermal-expansion analysis of the work roll during rolling*, Journal of Materials Processing Technology 49 (1995), pp. 125–147.
- [48] J. Lagergren, *Friction evaluation in hot strip rolling by direct measurement in the roll gap of a model duo mill*, Journal of Materials Processing Technology 70 (1997), pp. 207–214.
- [49] C.H. Luo, *Modeling the frictional boundary conditions in a rolling process*, Journal of Materials Processing Technology 59 (1996), pp. 373–380.
- [50] M.N. Özisik *Finite Difference Methods in Heat Transfer*, CRC Press, 1994.
- [51] J. Thomas *Numerical Partial Differential Equations: Finite Difference Method*, Springer, 1995.
- [52] D. Wild, T. Meurer, and A. Kugi, *Modelling and experimental model validation for a pusher-type reheating furnace*, Mathematical and Computer Modelling of Dynamical Systems 15 (2009), pp. 209–232.
- [53] A. Steinboeck, D. Wild, T. Kiefer, and A. Kugi, *A mathematical model of a slab reheating furnace with radiative heat transfer and non-participating gaseous media*, International Journal of Heat and Mass Transfer 53 (2010), pp. 5933–5946.